

AD-A070 795

IOWA UNIV IOWA CITY DEPT OF PHYSICS AND ASTRONOMY

F/G 4/1

A CORRELATION BETWEEN AURORAL KILOMETRIC RADIATION AND INVERTED--ETC(U)

JAN 79 J L GREEN, D A GURNETT, R A HOFFMAN

N00014-76-C-0016

UNCLASSIFIED

U. OF IOWA-79-2

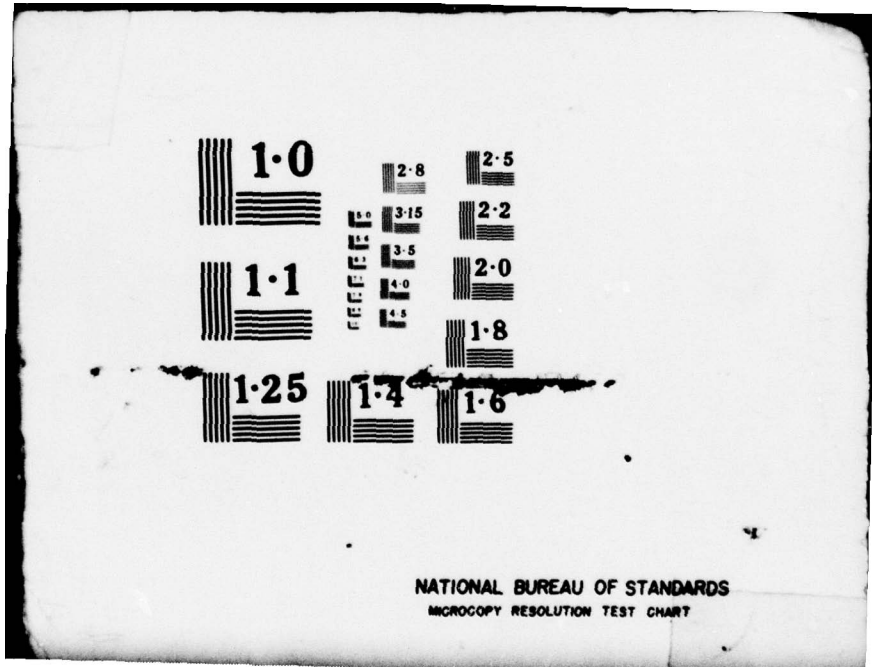
NL

| OF |
AD
A070795



END
DATE
FILMED

8-79
DDC

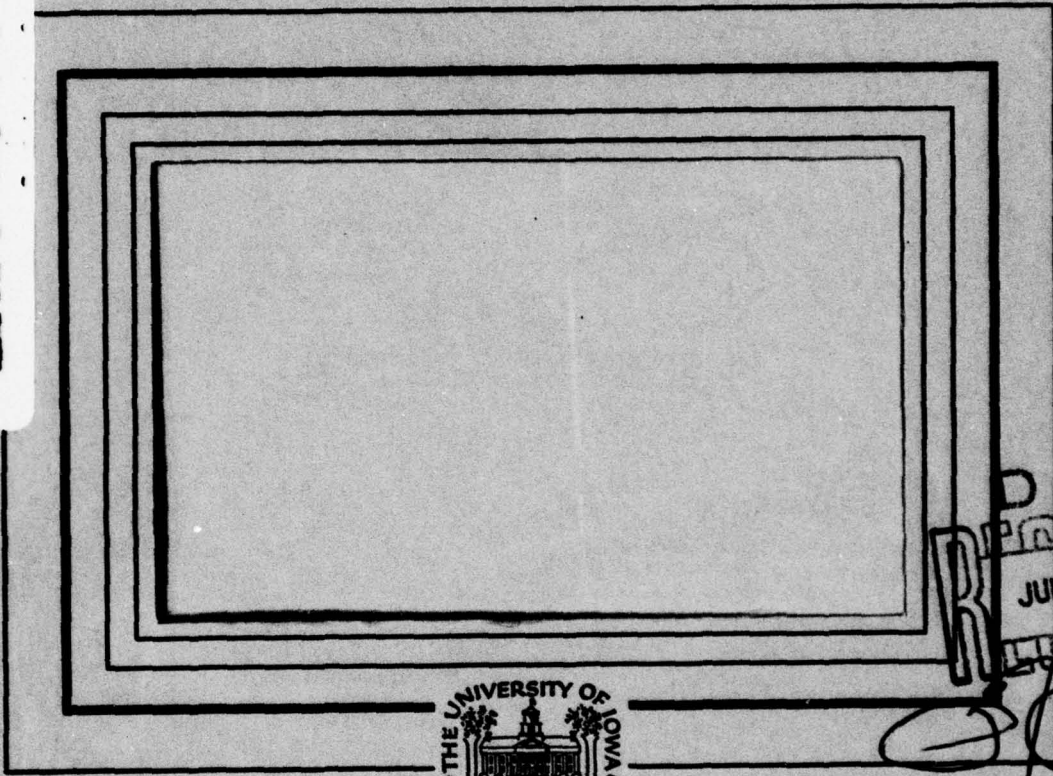


NATIONAL BUREAU OF STANDARDS
MICROCOPY RESOLUTION TEST CHART

LEVEL ¹⁴

(12)

ADA 070795



DDC
JUL 5 1979



DDC FILE COPY.

This document has been approved for public release and sale; its distribution is unlimited.

Department of Physics and Astronomy
THE UNIVERSITY OF IOWA

Iowa City, Iowa 52242

79 114 125 133

12

U. of Iowa-79-2

14

6
A Correlation Between
Auroral Kilometric Radiation
and
Inverted-V Electron Precipitation

by

10 James Lauer/Green*, Donald A./Gurnett†,
and Robert A./Hoffman†

DDC
RECEIVED
JUL 5 1979
RECEIVED

9 Progress rept.,

11 January, 1979

12447

* Department of Physics and Astronomy, The University
of Iowa, Iowa City, Iowa 52242, USA

+ Goddard Space Flight Center, Code 625, Greenbelt,
Maryland 20771, USA

This document has been approved
for public release and sale; its
distribution is unlimited.

Submitted to J. Geophys. Res.

The research at the University of Iowa was supported by NASA
under Grant NGL-16-001-043 and Contract NAS1-13129 and by the Office
of Naval Research Contract N00014-76-C-0016,

15 NAS1-13129

188 460 mt

UNCLASSIFIED

SECURITY CLASSIFICATION OF THIS PAGE (When Data Entered)

REPORT DOCUMENTATION PAGE		READ INSTRUCTIONS BEFORE COMPLETING FORM
1. REPORT NUMBER U. of Iowa-79-2	2. GOVT ACCESSION NO.	3. RECIPIENT'S CATALOG NUMBER
4. TITLE (and Subtitle) A CORRELATION BETWEEN AURORAL KILOMETRIC RADIATION AND INVERTED-V ELECTRON PRECIPITATION		5. TYPE OF REPORT & PERIOD COVERED Progress, January, 1979
7. AUTHOR(s) J. L. Green, D. A. Gurnett, and R.A. Hoffman		6. PERFORMING ORG. REPORT NUMBER
9. PERFORMING ORGANIZATION NAME AND ADDRESS Department of Physics and Astronomy The University of Iowa Iowa City, IA 52242		8. CONTRACT OR GRANT NUMBER(s) N00014-76-C-0016
11. CONTROLLING OFFICE NAME AND ADDRESS Electronics Program Office Office of Naval Research Arlington, VA 22217		10. PROGRAM ELEMENT, PROJECT, TASK AREA & WORK UNIT NUMBERS
14. MONITORING AGENCY NAME & ADDRESS (if different from Controlling Office)		12. REPORT DATE January, 1979
		13. NUMBER OF PAGES 27
		15. SECURITY CLASS. (of this report) UNCLASSIFIED
		15a. DECLASSIFICATION/DOWNGRADING SCHEDULE
16. DISTRIBUTION STATEMENT (of this Report) Approved for public release; distribution is unlimited.		
17. DISTRIBUTION STATEMENT (of the abstract entered in Block 20, if different from Report)		
18. SUPPLEMENTARY NOTES		
19. KEY WORDS (Continue on reverse side if necessary and identify by block number) Auroral Kilometric Radiation Inverted-V Electron Precipitation		
20. ABSTRACT (Continue on reverse side if necessary and identify by block number) [See page following]		

DD FORM 1473
1 JAN 73EDITION OF 1 NOV 68 IS OBSOLETE
S/N 6102-014-6601

UNCLASSIFIED

SECURITY CLASSIFICATION OF THIS PAGE (When Data Entered)

ABSTRACT

Simultaneous observations of energetic electron precipitations and auroral kilometric radiation (AKR) were obtained from the polar orbiting satellites AE-D and Hawkeye. The Hawkeye observations were restricted to periods when the satellite was in the AKR emission cone in the northern hemisphere and at radial distances $> 7 R_E$ to avoid local propagation cutoff effects. In addition, the AE-D measurements were restricted to complete passes across the auroral oval in the evening to midnight local time sector (from 20 to 01 hours magnetic local time). This is the local time region where the most intense bursts of AKR are believed to originate.

A qualitative survey of AKR and electron particle precipitation shows that AKR is more closely associated with inverted-V electron precipitation than with plasma sheet precipitation. Quantitatively, a good correlation is found between the AKR intensity and the peak energy of inverted-V events. In addition, in the tail of the most field-aligned portion ($\sim 0^\circ$ pitch angle) of the distribution functions of the inverted-V events, systematic changes are indicated as the associated AKR intensity increases. When the AKR power flux is weak ($< 10^{-17}$ watts/(m²Hz)) the effective tail temperature ($T_{||}$) in $F(V_{||})$ of the inverted-V events is less than 1.8×10^8 K while for $T_{||}$ greater

than 1.8×10^8 °K the associated AKR power flux is moderate (10^{-17} to 10^{-15} w/(m²Hz)) to intense ($> 10^{-15}$ w/(m²Hz)). From a determination of the simultaneous power in the inverted-V events and the AKR bursts, the efficiency of converting the charge particle energy into EM radiation increases to a maximum of about 1% for the most intense AKR bursts. However, conversion efficiencies as low as $10^{-5}\%$ are also found. There is some evidence which suggests that the tail temperature, $T_{||}$ in $F(V_{||})$ of the inverted-V events, may play an important role in the efficient generation or amplification of auroral kilometric radiation.

Accession For		<input checked="" type="checkbox"/>
WHS GRAD		<input type="checkbox"/>
DSC TAB		<input type="checkbox"/>
Unannounced		
Justification		
By _____		
Dist. to _____		
Avail. to _____		
Dist	Avail. and/or special	
A		

I. INTRODUCTION

Auroral kilometric radiation (or AKR) is the most intense electromagnetic radiation that is generated by the earth's magnetosphere at kilometric wavelengths. The origin of this radiation has been difficult to determine since AKR is extremely sporadic and can vary in intensity by as much as 80 db on a time scale of minutes and possibly seconds. A recent study by Gallagher and Gurnett [1979], however, demonstrates quite clearly that the intense AKR is generated on the average, at low altitude (from 2 to 3 earth radii) between 22 and 24 hours magnetic local time in the auroral zone. This determination of the source region of auroral kilometric radiation agrees extremely well with the previous published results of Gurnett [1974] and Kurth et al. [1975] and corresponds to the "region of frequent TKR activity" determined by Alexander and Kaiser [1976].

A considerable amount of indirect evidence indicates that AKR is generated by auroral particle precipitation during geomagnetic substorms. For instance, the intense AKR has been correlated with high-latitude magnetic disturbances produced by the auroral electrojet current as measured by the AE index (see for example, Voots et al. [1977]). In addition, a close association between AKR and discrete auroral arcs was demonstrated by Gurnett [1974] and Kurth et al. [1975].

Gurnett concluded that AKR is associated with inverted-V electron precipitation since Ackerson and Frank [1972] had previously shown that inverted-V electron precipitation events are correlated with discrete auroral arcs.

The purpose of this paper is to show the direct relationship between the AKR power flux observed by the eccentric orbiting Hawkeye spacecraft and energetic electron precipitation in the nighttime auroral zone measured by the low altitude polar orbiting AE-D spacecraft. The Hawkeye plasma and radio wave experiment has been described by Kurth et al. [1975], and the AE-D Low-Energy Electron experiment has been described by Lin and Hoffman [1979].

II. METHOD OF ANALYSIS

The simultaneous observations presented in this paper from Hawkeye and AE-D reveal many important characteristics of auroral kilometric radiation that cannot be discerned from a single spacecraft. One of the most important questions which can be investigated is what are the energies of the particles which play a major role in the generation of AKR. To determine such a particle distribution requires in situ observations of the precipitating auroral particles at relatively low altitudes in the region where the radiation is generated. Remote electric field measurements are required to obtain an integrated power flux measurement of auroral kilometric radiation from the pre-midnight active auroral region. These requirements necessitate the use of two widely separated satellites, one at low altitudes (AE-D) and the other (Hawkeye) far from the earth. To do a statistically meaningful study of this type requires rigid constraints on the time of the observations and constraints on the satellites' positions because of the localization of the source region of auroral kilometric radiation and the propagation characteristics of the radiation.

A. Constraints On the AE-D Observations

AE-D was launched on October 6, 1975, into a polar orbit with initial apogee and perigee of 4,000 km and 150 km, respectively, and inclination of 90°. During its brief 4 month lifetime, the

Low Energy Electron (LEE) experiment measured electron fluxes in 16 energy channels ranging from 200 eV to 25 keV in a one-second instrument cycle. Each of the Low Energy Electron detectors has an acceptance angle of about 15° and an energy acceptance band ($\Delta E/E$) of 30%.

Lin and Hoffman [1979] have shown that inverted-V electron precipitations observed by the LEE experiment onboard AE-D are found at all local times not only in the auroral zone, but in the polar cap region as well. In contrast, Gallagher and Gurnett [1979] and others have determined that the most intense bursts of auroral kilometric radiation originate from 22 to 24 hours magnetic local time at high latitudes (greater than 57° invariant latitude). There are, however, several characteristics which distinguish the inverted-V electron precipitations in the local evening (from about 19 hours to 01 hour magnetic local time) from those observed at other local times. Lin and Hoffman [1979] determined that the inverted-V events observed in the local evening are on the average much broader in invariant latitude and the characteristic peak energies of the events are on the average higher than those at other local times. For the purposes of this study, only the AE-D observations from 20 hours to 01 hour magnetic local time will be used since this is the region where the most intense bursts of auroral kilometric radiation are believed to originate and the most energetic inverted-V events are observed.

B. Constraints On the Hawkeye Observations

Hawkeye was in a highly eccentric earth orbit with an apogee radial distance of nearly $22 R_E$ (earth radii) in the northern hemisphere and inclination of about 89° . This spacecraft provided continuous observations of AKR for long periods of time (up to 46 hours per 52 hour orbit) from launch on June 3, 1974, until reentry on April 28, 1978. This enabled Green et al. [1977] to determine the angular distribution of auroral kilometric radiation at several frequencies from a frequency of occurrence survey. Green et al. [1977] found that at 178 kHz the highest probability of observing AKR occurs at magnetic latitudes $\geq 60^\circ$ on the dayside of the earth, but is as low as 20° on the nightside. The region of magnetic latitude and magnetic local time where Hawkeye has the highest probability of observing auroral kilometric radiation (black shading in Figure 4 of Green et al. [1977]) was termed the AKR emission cone. In addition, from simultaneous observations from IMP-8 and Hawkeye and ray tracing in a model magnetosphere Green et al. [1977] concluded that the topside plasmasphere on the nightside produces an abrupt latitudinal propagation cutoff to the radiation and prevents auroral kilometric radiation generated in the southern hemisphere from being observed in the northern hemisphere.

In order to insure that Hawkeye has the highest probability of observing auroral kilometric radiation, if it is being generated, the Hawkeye observations used in this study are selected from the

times when Hawkeye was in the AKR emission cone and at radial distances $\geq 7 R_E$ to avoid local propagation cutoff effects. The simultaneous AKR power flux measurements and AE-D particle observations used in this study are taken from the times when both satellites were in the northern hemisphere.

III. QUALITATIVE COMPARISON OF AKR AND AURORAL PARTICLE PRECIPITATION

During the 4 months that Hawkeye and AE-D were simultaneously in orbit there were 93 passes which met the criterion outlined in the previous two sections. Figure 1 is a qualitative comparison of some typical events. The top panel of Figure 1 shows the electric field intensities detected by Hawkeye at 178 kHz while it is in the AKR emission cone. All these enhanced radio emissions are attributed to auroral kilometric radiation. During this period of Hawkeye observations, AE-D transversed the nighttime auroral oval in the northern hemisphere on three consecutive passes. The energy-time spectrograms from the Low Energy Electron array of stepped detectors on AE-D are shown in the bottom three panels labeled orbits 698, 699, and 700. In the first two auroral passes, orbits 698 and 699, the AE-D spacecraft was in the de-spin mode where the spin period was one revolution per orbit. During these two passes, the stepped electron detectors had a view angle of -7° to the radius vector and, thus, were looking at precipitating electrons with pitch angles of less than 11° . The bottom panel, orbit 700, corresponds to a period when the AE-D spacecraft was in a spinning mode with a spin period of 15 seconds.

Inverted-V electron precipitation events are characterized by electron fluxes which increase from a few hundred eV to keV energies and then return to a few hundred eV energies as the spacecraft crosses this narrow band of auroral electron precipitation. This type of precipitation creates an inverted-V shaped intensity band in energy-time spectrograms [Frank and Ackerson, 1971]. On orbit 698 in Figure 1, the Low Energy Electron detectors on AE-D measured three energetic inverted-V electron precipitation events at 1102, 1102:15 and 1102:30 UT with peak energies of 1.9 keV, 1.38 keV and 13.1 keV. Approximately two hours later, on the next pass through the auroral oval in the northern hemisphere, the Low Energy Electron experiment measured at least two energetic inverted-Vs with peak energies of 6.88 keV and 3.62 keV plus moderately intense electron plasma sheet precipitation. Simultaneously, the Hawkeye plasma wave experiment measured moderately intense bursts of auroral kilometric radiation at 178 kHz in excess of 10^{-16} watts/ (m^2Hz) (see arrows labeled 698 and 699 in top panel of Figure 1). Much of the electron precipitation referred to here as plasma sheet precipitation has the same characteristics that Winningham et al. [1975] described as coming from the central plasma sheet region of the magnetotail and corresponds to regions of diffuse aurora. The plasma sheet precipitation has large electron fluxes at low energies extending in latitude to as much as 10° and is quite easily distinguishable from inverted-V events in the energy time spectrograms. On orbit 700 moderately intense electron plasma sheet precipitation is observed by AE-D while no evidence of inverted-V precipitation is

found. The spin modulation of the electron fluxes in the bottom panel indicates the precipitating nature of these electrons. No auroral kilometric radiation is detected during the last AE-D auroral pass (arrow labeled 700) in Figure 1.

The results of the qualitative survey of simultaneous observations of auroral kilometric radiation and electron precipitation in the nighttime auroral oval are summarized in Table 1. The Hawkeye observations are classified according to whether or not auroral kilometric radiation is detected above the noise level of the plasma wave instrument. The electron measurements are classified according to all possible combinations of two basic types of electron precipitation patterns measured by AE-D in the nighttime auroral oval; inverted-V and plasma sheet precipitation. Energetic inverted-V precipitation and no plasma sheet precipitation (see the E-t spectrogram from orbit 698 in Figure 1 as an example) occurred on 15% of the simultaneous observations and Hawkeye always detected AKR at those times. During 49% of the auroral zone passes where AE-D observed inverted-V and electron plasma sheet precipitation (see the E-t spectrogram of orbit 699 as an example) Hawkeye detected auroral kilometric radiation. However, on two auroral passes (2% of the time) when AE-D observed energetic particle precipitation in the form of inverted-V and plasma sheet precipitation, Hawkeye did not detect AKR. AE-D observed electron plasma sheet precipitation and no inverted-V precipitation on 25% of the simultaneous observations (see the orbit 700 E-t spectrogram in

Figure 1 as an example) while Hawkeye did not observe auroral kilometric radiation above the receiver's noise level. The plasma sheet precipitation on seven of these AE-D auroral passes when Hawkeye did not detect AKR had intense energy fluxes $> 10^8$ keV/(sec cm² ster) (comparable to the energy fluxes in many of the inverted-V events). This qualitative survey supports the conclusion of Gurnett [1974] that auroral kilometric radiation is more closely associated with inverted-V electron precipitation than with plasma sheet precipitation in the nighttime auroral zone.

If auroral kilometric radiation is generated by precipitating inverted-V electrons, then an explanation must be sought for the cases in which AKR was detected when AE-D observed plasma sheet precipitation and no inverted-V precipitation (9% of the time). Quite obviously the AE-D detectors do not survey the nature of the particle precipitation over the entire pre-midnight active auroral region in one pass. Since the precipitation pattern of inverted-V events, like discrete auroral arcs, does vary considerably in local time it is reasonable to assume that inverted-V structures could be missed.

IV. QUANTITATIVE ANALYSIS OF AKR AND INVERTED-V EVENTS

It is of importance to explore more quantitatively any relationship between auroral kilometric radiation and energetic inverted-V electron precipitation if indeed these particles are the ultimate source of energy for this electromagnetic radiation. If auroral kilometric radiation and inverted-V events are correlated, as suggested by Figure 1 and Table 1, then it is reasonable to expect that as the energy in the inverted-V events increases, so might the intensity of the kilometric radiation. Figure 2 is a scatter plot of simultaneous three minute average AKR power flux measurements at 178 kHz versus the inverted-V peak energy which is used here to characterize the particle energy in the event. A three minute averaged power flux measurement takes into account any spin modulation effect and gives an electric field measurement on a time scale comparable with the complete crossing of AE-D across the auroral oval. A $1/R^2$ correction is applied to the average power flux measurements to take into account the radial dependence of this radiation. The variable R is the distance from the satellite to the average source region of the most intense bursts of AKR ($2.5 R_E$ geocentric radial distance at an L value of 8.55 and a magnetic local time of 23 hours in agreement with Gallagher and Gurnett [1979]).

In addition, the intensities have been normalized to a radial distance of $7 R_E$. The two triangles represent the minimum detectable signals by Hawkeye since no AKR was detected at those times. During AE-D passes where several inverted-V events were observed, only the event with the largest peak energy is plotted. The peak energy is the center energy of the channel where the peak particle flux associated with the inverted-V event is observed. There appears to be an obvious relationship between these two parameters, that is, as the mean of the AKR power flux measurements increase so does the characteristic peak energy of the precipitating inverted-V. This is valid up to about 18 keV where the relationship appears to reverse, but too few points are available for a definite trend at high energies to be clearly established. Statistically, below 18 keV the linear correlation coefficient of the log (power flux) versus the peak energy is 0.70. A random error analysis shows that this corresponds to a greater than 99.99% probability that these two parameters are related.

An examination of the distribution functions at $\sim 0^\circ$ pitch angle at the time of the peak in the inverted-V events used in Figure 2 reveal striking differences when ordered by increasing magnitude of the simultaneous power flux observations of auroral kilometric radiation. The distribution function at 0° pitch angle is the most field-aligned part assuring us of examining electrons of magnetospheric origin which have been presumably accelerated down to AE-D altitudes and possibly through the AKR source region (see Discussion). Figure 3 shows three representative electron

distribution functions when Hawkeye observed weak (top panel), moderate (center panel), and intense (bottom panel) auroral kilometric radiation in the AKR emission cone. The actual power flux measurements associated with the AE-D observations of Figure 3 are given in the upper right corner of each panel. The electron distribution functions $F(V_{||})$ of Figure 3 are calculated from the observed differential fluxes J at energies E by

$$F(V_{||}) = \frac{m_e^2}{2} \frac{J}{E} = 1.616 \times 10^{-7} \frac{J}{E}$$

with

$F(V_{||})$ in electrons sec^3/km^6 ,

J in $\frac{\text{electrons}}{\text{cm}^2 \text{sec ster keV}}$,

E in keV,

m_e equals the electron mass in kg.

A major difference between the distribution functions in Figure 3, as suggested by Figure 2, is that the peak in each inverted-V event increases as the AKR power flux associated with the event increases. The peaks of the inverted-V events in the top, center, and bottom panels occur at parallel velocities of about 3×10^4 , 4×10^4 , and

6.7×10^4 km/sec, respectively. In general, for the times when Hawkeye observes weak auroral kilometric radiation $< 10^{-17}$ watts/(m²Hz)(normalized to $7 R_E$) the peaks of the inverted-V events observed by AE-D have values of $F(V_{||})$ that range from 1.0 electron sec³/km⁶ to as high as 40 electrons sec³/km⁶ and are easily distinguishable in the $F(V_{||})$ distributions (see for example top panel of Figure 3). In contrast, when Hawkeye observes very intense auroral kilometric radiation $> 10^{-14}$ watts/(m²Hz)(normalized to $7 R_E$) the value of $F(V_{||})$ at the peak of the inverted-V events range from 0.1 to 4.0 electrons sec³/km⁶ with the peaks almost indistinguishable from a plateau like structure in these distribution functions. A plateau or horizontal flattening in $F(V_{||})$ at large velocities (see for example the bottom panel in Figure 3 from 2×10^4 to 6×10^4 km/sec) is a common feature for the distribution functions associated with power fluxes of auroral kilometric radiation $> 10^{-15}$ watts/(m²Hz) (normalized to $7 R_E$). The slope of the plateau or tail in the distribution functions can be quantitatively determined by calculating an effective tail temperature given by

$$T_{||} = \frac{m_e}{k_B} \frac{\int_{V_A}^{V_B} v_{||}^2 F(v_{||}) dv_{||}}{N}$$

where

k_B equals Boltzmann's constant,

V_A equals 4×10^4 km/sec,

V_B equals 8×10^4 km/sec, and

$$N = \text{density} = \int_{V_A}^{V_B} F(V_{\parallel}) dV_{\parallel} \quad .$$

The quantity T_{\parallel} is an effective temperature since calculation of the temperature requires knowledge of the distribution function at all velocities plus knowledge of any streaming in the distribution. Figure 4 is a scatter plot of the power flux measurements of auroral kilometric radiation versus the effective tail temperature T_{\parallel} in the distribution functions at $\sim 0^\circ$ pitch angle of the inverted-V events simultaneously observed by AE-D. The integration limits for calculating T_{\parallel} are determined such that at the high velocity (high energy) limit the observed fluxes for all the inverted-V events are above the threshold of the LEE detectors and the lower velocity (low energy) limit is above major inverted-V peaks in the distribution functions. The correlation coefficient in Figure 4 between the log of the power flux and the effective tail temperature (T_{\parallel}) is 0.49. Even though this is a relatively low linear correlation coefficient when the AKR power flux is weak ($< 10^{-17}$ watts/(m²Hz)) T_{\parallel} is less than 1.8×10^8 °K while for T_{\parallel} greater than 1.8×10^8 °K the associated AKR power flux is moderate (10^{-17} to 10^{-15} watts/(m²Hz)) to intense ($> 10^{-15}$ watts/(m²Hz)).

Figure 5 is a scatter plot of three minute average AKR power flux measurements versus the energy flux at the time of the peak in precipitating inverted-V events used in Figures 2 and 4. The energy flux is determined from numerically integrating the energy (E) of the precipitating electrons times the differential flux (J) at that energy over the energy range of the Low Energy Electron detectors (200 eV to 25 keV).

$$\text{ENERGY FLUX} = \int_{0.2 \text{ keV}}^{25 \text{ keV}} EJdE$$

The additional vertical scale in Figure 5 (right hand side) is for the corresponding AKR total power output derived from the Hawkeye power flux measurements and from previous knowledge of the time-averaged AKR bandwidth of 200 kHz [Kaiser and Alexander, 1977] and the angular distribution of the radiation of 3.5 steradians [Green *et al.*, 1977]. The top scale is the amount of total power in the precipitating inverted-V events (not counting plasma sheet precipitation) and is derived from the actual measured particle fluxes and assumed average latitudinal width of 1.5° for these events as recently reported by Lin and Hoffman [1979] and an estimated longitudinal width of 75° (from 20 hours to 01 hour magnetic local time) which is a typical longitudinal extent of a discrete auroral arc. The far right vertical scale and the top horizontal scale are only used as rough estimates of the AKR and charged particle power

in these events since simultaneous measurements of all the parameters necessary to determine these values is not possible.

A direct horizontal mapping of the data in Figure 2 can be made to Figure 5. Inverted-V events with large energy fluxes $\approx 10^{10}$ keV/(sec cm² ster) have characteristic peak energies ranging from 2.62 keV to 24.9 keV, but the most intense bursts of AKR are associated with inverted-V events which have peak energies ≥ 7 keV. This mapping indicates that even though there may be $\geq 10^{10}$ watts of power in a precipitating inverted-V event it is not necessarily true that at the same time there will be intense kilometric radiation. It is then reasonable to assume that the generation of AKR may be very sensitive to other plasma parameters in the source region and special anisotropies in the distribution function of the precipitating particles.

Another important feature of Figure 5 is that if inverted-V precipitation is the ultimate energy source, the efficiency of converting the charge particle energy into electromagnetic radiation increases to a maximum of about 1% for the most intense AKR bursts. This result is in excellent agreement with earlier estimates. As Figure 5 illustrates, however, a 1% efficiency occurs in only a few percent of the cases. The median of the distribution in Figure 5 is at about 0.001% efficiency with the lowest conversion efficiency near $10^{-5}\%$.

V. DISCUSSION

A qualitative survey of auroral kilometric radiation and electron particle precipitation in the nighttime auroral oval has shown that auroral kilometric radiation is more closely associated with inverted-V electron precipitation than with plasma sheet precipitation. A statistical analysis of the AKR intensity and the characteristic peak energies of inverted-V events simultaneously measured indicates that below 18 keV they are well correlated (with a correlation coefficient of 0.70). Several sources of errors and fluctuations could have contributed to the scatter in Figure 2 (also in Figures 4 and 5) which we will presently discuss. There are no detailed studies of the distribution of intensity in the AKR emission cone. Without this information it is not known whether some of the Hawkeye observations were from times when it was in a slight intensity hole or depression in the emission cone. However, simultaneous plasma wave observations by Hawkeye and IMP-6 were presented by Green et al. [1977] which illustrate that bursts of auroral kilometric radiation do illuminate large regions of the AKR emission cone with comparable intensities indicating that this may not contribute extensively to the scatter in Figure 2. If the source region of an AKR storm was different than the average source position (see section IV)

used in the $1/R^2$ correction to the intensity then this would contribute to the error. Any difference in actual source position from the average source used in this survey would introduce a relatively small error of a few db if the AKR source remained in the nighttime auroral zone. The peak in the emission spectrum of auroral kilometric radiation has been observed by Kaiser and Alexander [1977] to decrease with increasing AE. This change in the peak frequency could produce an increase in the power flux at 178 kHz since the 178 kHz channel is near the spectral peak. The enhancement at 178 kHz due to this effect could produce a maximum increase of less than one order of magnitude. Another point to consider is that since AE-D cuts through the nighttime auroral oval at nearly constant local time it is certain that AE-D will not always observe the most intense part of the electron precipitation pattern. The maximum altitude of AE-D during the particle observations used in this study was nearly 1000 km which is believed to be several thousand kilometers below the average source region of auroral kilometric radiation at 178 kHz [see Gallagher and Gurnett, 1979]. Great changes can occur in the pitch angle distribution, loss cone angle, and inverted-V peak of the electron distribution function due to the mirroring effect alone (conservation of the first adiabatic invariant). The mirroring effect on the distribution function at $\sim 0^\circ$ pitch angle is greatly reduced for the precipitating particles used in this study. The correlation between auroral kilometric

radiation and the peak energies of precipitating inverted-V events as shown in Figure 2 is relatively good despite the problems outlined above.

It is important to note that Figure 5 is very similar to the correlation of AKR intensity with the AE index [Figure 5 of Voots et al., 1977]. AE is directly proportional to the auroral electrojet current and is believed to be fed by field-aligned currents flowing into and out of the ionosphere in the auroral zones. Figure 5 from Voots et al. [1977] shows that during times of large excursions of the AE index ($\sim 1000 \gamma$) a large range of intensities of AKR have been observed (from 10^{-20} to 10^{-14} watts/(m²Hz) normalized to $30 R_E$). However, for times when AE index is below 158γ 68.7% of the power flux measurements are below 6.31×10^{-19} watts/(m² Hz). Figure 5 in a similar way illustrates that at times when large amounts of power are present in precipitating inverted-V events there is a large range in the observed intensity of AKR bursts (from 10^{-18} to 10^{-13} watts/(m² Hz) normalized to $7 R_E$). Inverted-V events with peak energies ≥ 7 keV and with energy fluxes $> 10^9$ keV/(sec cm² ster) are associated with the most intense bursts of auroral kilometric radiation. Figure 5 and Figure 5 from Voots et al. [1977] suggest that it is not sufficient to have large amounts of power available in the charged particles precipitating in the auroral zone for the simultaneous production of intense auroral kilometric radiation, but in addition to the power requirements, special features

or anisotropies in the particle distribution function or in the plasma parameters in the source region are needed for the instability to obtain high efficiencies.

Figure 4 suggests that the tail temperature $T_{||}$ of $F(V_{||})$ may be a special feature of the distribution function needed for the efficient generation or amplification of auroral kilometric radiation. Many of the inverted-V events that are associated with weak to moderate AKR ($< 10^{-16}$ watts/(m²Hz)) have large energy fluxes (from 10^9 to 10^{10} keV/(sec cm² ster) of Figure 5) because they are observed to have very large differential fluxes at low energies and very small differential fluxes at high energies (small $T_{||}$). The inverted-V events that are associated with intense AKR ($> 10^{-14}$ watts/(m²Hz)) have relatively small differential fluxes at low energies but moderately large fluxes at high energies (large $T_{||}$). To illustrate this effect on the calculation of the energy flux Figure 6 is a similar scatter plot to Figure 5 except the lower limit of integration has been changed from 0.2 keV (as in Figure 5) to 6.88 keV. The inverted-V events in Figure 6 with energy fluxes less than 10^8 keV/(sec cm² ster) had comparatively small tail temperatures and are associated with weak to moderate auroral kilometric radiation ($< 10^{-15}$ watts/(m²Hz)). In contrast, these data in Figure 5 had energy fluxes greater than 10^8 keV/(sec cm² ster) illustrating that these inverted-V events were observed to have high electron differential fluxes at low energies (< 6.88 keV). In addition, the most intense bursts of auroral kilometric radiation ($> 10^{-14}$ watts/(m²Hz)) in Figure 5 and Figure 6 were

associated with inverted-V events with energy fluxes greater than 10^9 keV/(sec cm² ster) illustrating that these inverted-V events had large electron differential fluxes in the tail of $F(V_{||})$ and comparatively large $T_{||}$. If the tail of the distribution function $F(V_{||})$ of inverted-V events is important for the amplification of auroral kilometric radiation through, for example, a possible resonance interaction, then Figure 6 illustrates that in some cases efficiencies as high as 0.1 to 1% may be possible for a dynamic range in AKR intensity as large as 80 db. There are, however, serious difficulties with this suggestion since there are many data points in Figure 6 which show that weak AKR bursts are associated with intense particle precipitations and large differential fluxes at high energies in the tail of $F(V_{||})$. Resolution of these difficulties may have to wait until the launch of Dynamics Explorer in 1980 since this spacecraft may be able to make simultaneous observations of AKR and particle distributions in the source region of auroral kilometric radiation.

The results of this study show that auroral kilometric radiation is more closely associated with inverted-V electron precipitation than with plasma sheet precipitation. In addition, there is evidence that suggests that the efficiency of generating auroral kilometric radiation from inverted-V particle precipitation ranges from $10^{-5}\%$ to a maximum efficiency of about 1%. Any realistic theory on the generation of auroral kilometric radiation must account for such a wide range in efficiencies.

ACKNOWLEDGEMENTS

We are very grateful to Ron Janetzke and coworkers at Goddard Space Flight Center for their efforts in making the AE-D data quickly available. In addition, special thanks are due David Barbosa for the many stimulating discussions and suggestions.

The research at the University of Iowa was supported by NASA under Grant NGL-16-001-043 and Contract NAS1-13129 and by the Office of Naval Research Contract N00014-76-C-0016.

REFERENCES

- Ackerson, K. L., and L. A. Frank, Correlated satellite measurements of low-energy electron precipitation and ground-based observations of a visible auroral arc, J. Geophys. Res., 77, 1128, 1972.
- Alexander, J. K., and M. L. Kaiser, Terrestrial kilometric radiation, I, Spatial structure studies, J. Geophys. Res., 81, 5948, 1976.
- Frank, L. A., and K. L. Ackerson, Observations of charged particle precipitation into the auroral zone, J. Geophys. Res., 76, 3612, 1971.
- Gallagher, D. L., and D. A. Gurnett, Auroral kilometric radiation: Time-averaged source location, (submitted for publication), J. Geophys. Res., 1979.
- Green, J. L., D. A. Gurnett, and S. D. Shawhan, The angular distribution of auroral kilometric radiation, J. Geophys. Res., 82, 1825, 1977.
- Gurnett, D. A., The earth as a radio source: Terrestrial kilometric radiation, J. Geophys. Res., 79, 4227, 1974.

Kaiser, M. L., and J. K. Alexander, Terrestrial kilometric radiation 3. Average Spectral Properties, J. Geophys. Res., 82, 3273, 1977.

Kurth, W. S., M. M. Baumbach, and D. A. Gurnett, Direction finding measurements of auroral kilometric radiation, J. Geophys. Res., 80, 2764, 1975.

Lin, C. S., and R. A. Hoffman, Characteristics of the Inverted-V Event, J. Geophys. Res., (to be published), 1979.

Voots, G. R., D. A. Gurnett, and S.-I. Akasofu, Auroral kilometric radiation as an indicator of auroral magnetic disturbances, J. Geophys. Res., 82, 2259, 1977.

Winningham, J. D., F. Yasuhara, S.-I. Akasofu, and W. J. Heikkila, The latitudinal morphology of 10-eV to 10-keV electron fluxes during magnetically quiet and disturbed times in the 2100 - 0300 MLT sector, J. Geophys. Res., 80, 3148, 1975.

FIGURE CAPTIONS

- Figure 1 Energy-time spectrograms from the LEE experiment on board AE-D showing electron precipitation during three consecutive passes across the nighttime auroral oval in the northern hemisphere. Note that AKR appears to be more closely related to inverted-V electron precipitation than to plasma sheet precipitation.
- Figure 2 Scatter plot of simultaneous measurements of AKR intensity (normalized to $7 R_e$ and having a $1/R^2$ correction) and the peak energy in inverted-V events observed by AE-D. Below 18 keV the correlation coefficient between the log of the power flux and the peak energy is 0.70. A random error analysis produces a probability of less than $10^{-5}\%$ in obtaining the 0.70 correlation coefficient from an uncorrelated parent population, illustrating the level of confidence for this correlation.
- Figure 3 Three electron distribution functions at $\sim 0^\circ$ pitch angle during the inverted-V events used in Figure 2. In the upper right corner of each panel is the simultaneous AKR power flux measurement from the Hawkeye spacecraft.

These three distribution functions are representative of the AE-D observations during times of weak (top panel), moderate (center panel), and intense (bottom panel) auroral kilometric radiation.

Figure 4 Scatter plot of the $1/R^2$ corrected AKR intensity at 178 kHz (normalized to $7 R_E$) and the effective tail temperature ($T_{||}$ defined in text) of the electron distribution functions at $\sim 0^\circ$ pitch angle of the inverted-V events used in Figure 2. The triangles represent times when auroral kilometric radiation was not detected above the receivers threshold. During times when the power flux is weak ($< 10^{-17}$ watts/(m^2 Hz)) $T_{||}$ is less than 1.8×10^8 °K. In addition, for $T_{||}$ greater than 1.8×10^8 °K the associated AKR power flux is moderate (10^{-17} to 10^{-15} watts/(m^2 Hz)) to intense ($> 10^{-15}$ watts/(m^2 Hz)).

Figure 5 Scatter plot of simultaneous measurements of AKR intensity at 178 kHz (normalized to $7 R_E$ and having a $1/R^2$ correction) and the energy flux of the same inverted-V events plotted in Figures 2 and 4. The top scale is an estimate of the amount of power available in the precipitating inverted-V events. The far right hand scale is an estimate of the amount of power in the AKR bursts. Note

that if the precipitating inverted-V events are the sole energy reservoir for AKR that the generation mechanism can have a maximum efficiency of about 1%.

Figure 6 Scatter plot of simultaneous measurements of AKR intensity at 178 kHz (normalized to $7 R_E$ and having a $1/R^2$ correction) versus the energy flux of the inverted-V events in Figure 5 integrated from 6.88 keV to 25 keV. A comparison with Figure 5 illustrates (but not conclusively) that the temperature of the tail in $F(V_{||})$ of the inverted-V events may play a role in the efficient generation of auroral kilometric radiation.

TABLE 1

		HAWKEYE ELECTRIC FIELD MEASUREMENTS	
		AKR Detected	No AKR Detected
AE-D electron measurements	Inverted-V precipitation and no plasma sheet precipitation	15%	0%
	Inverted-V and plasma sheet precipitation	49%	2%
	Plasma sheet precipitation and no inverted-V precipitation	9%	25%

The distribution of electric field measurements when Hawkeye is in the AKR emission cone as a function of AE-D precipitating electron measurements in the auroral oval from 20 hours to 01 hour magnetic local time. Percentages based on 93 simultaneous observations.

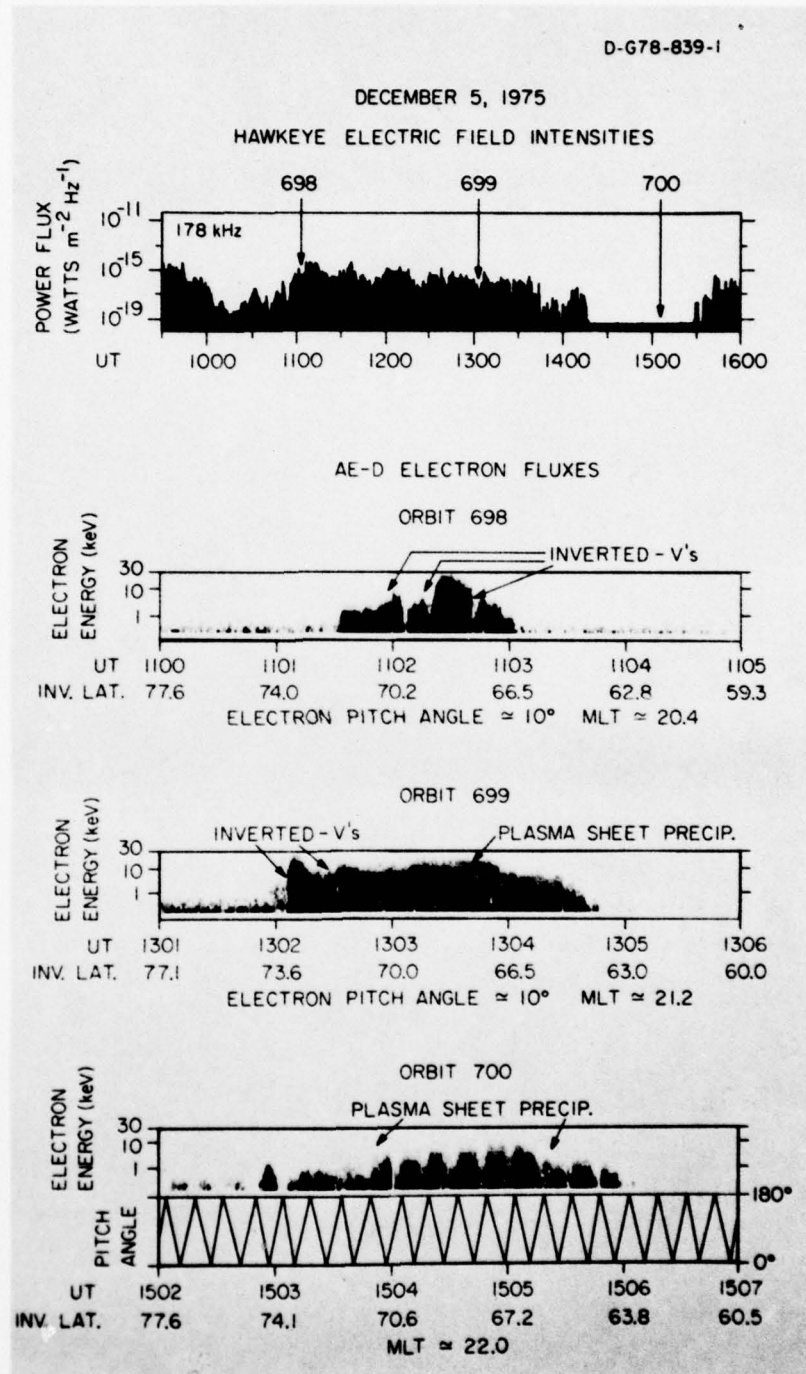


Figure 1

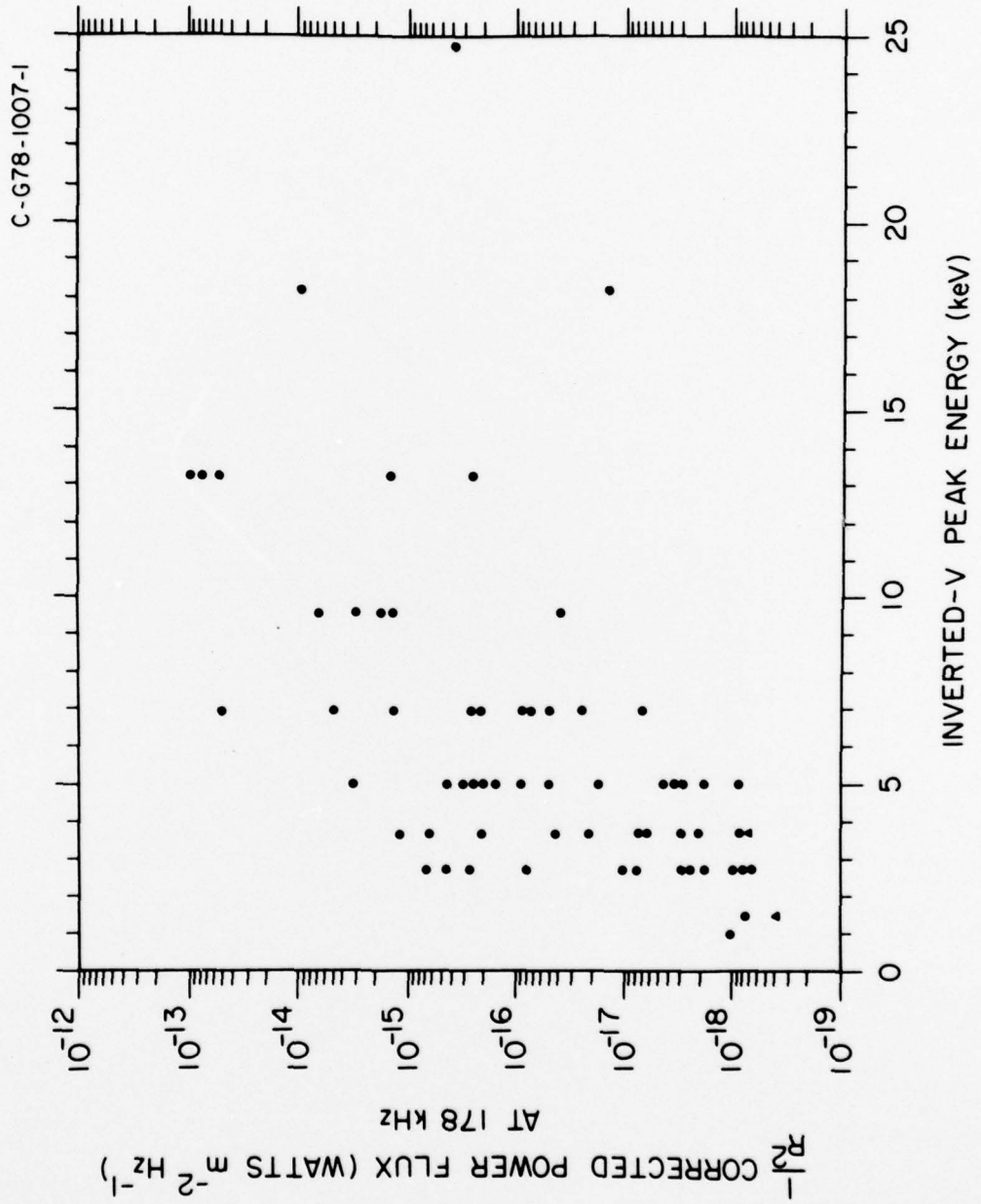


Figure 2

ELECTRON DISTRIBUTIONS AT $\sim 0^\circ$ PITCH ANGLE

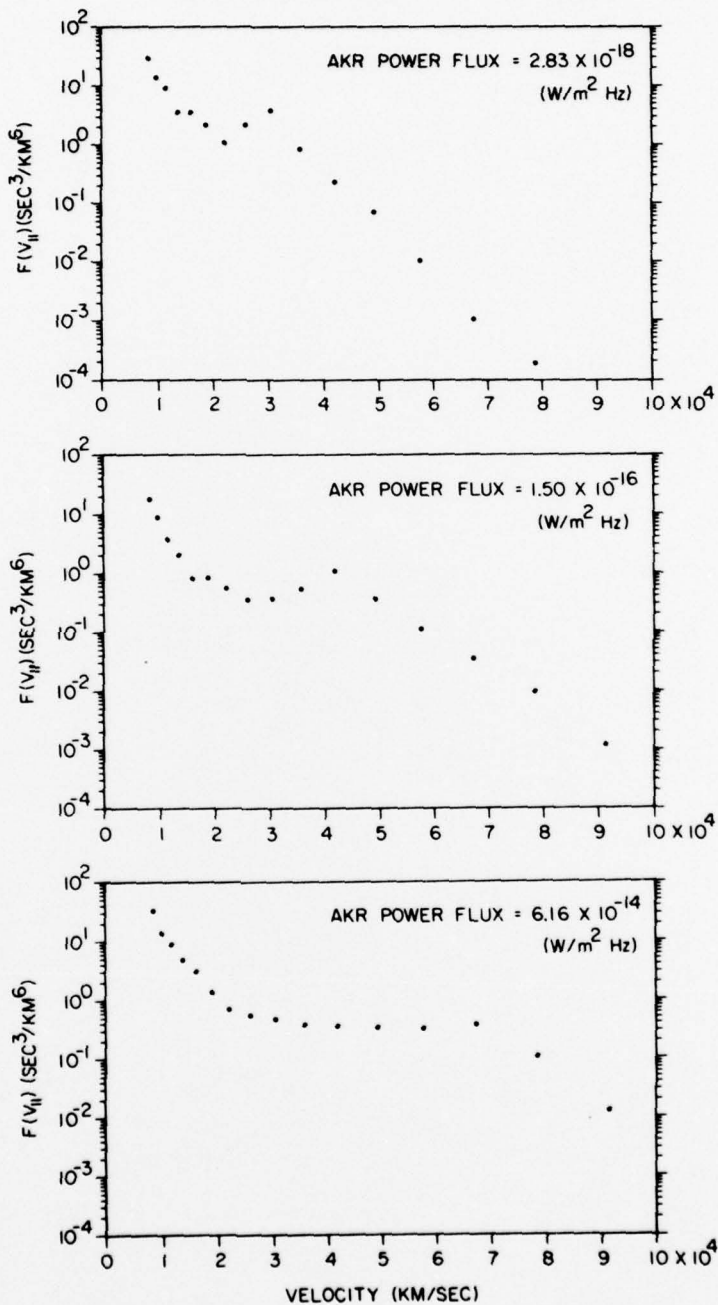


Figure 3

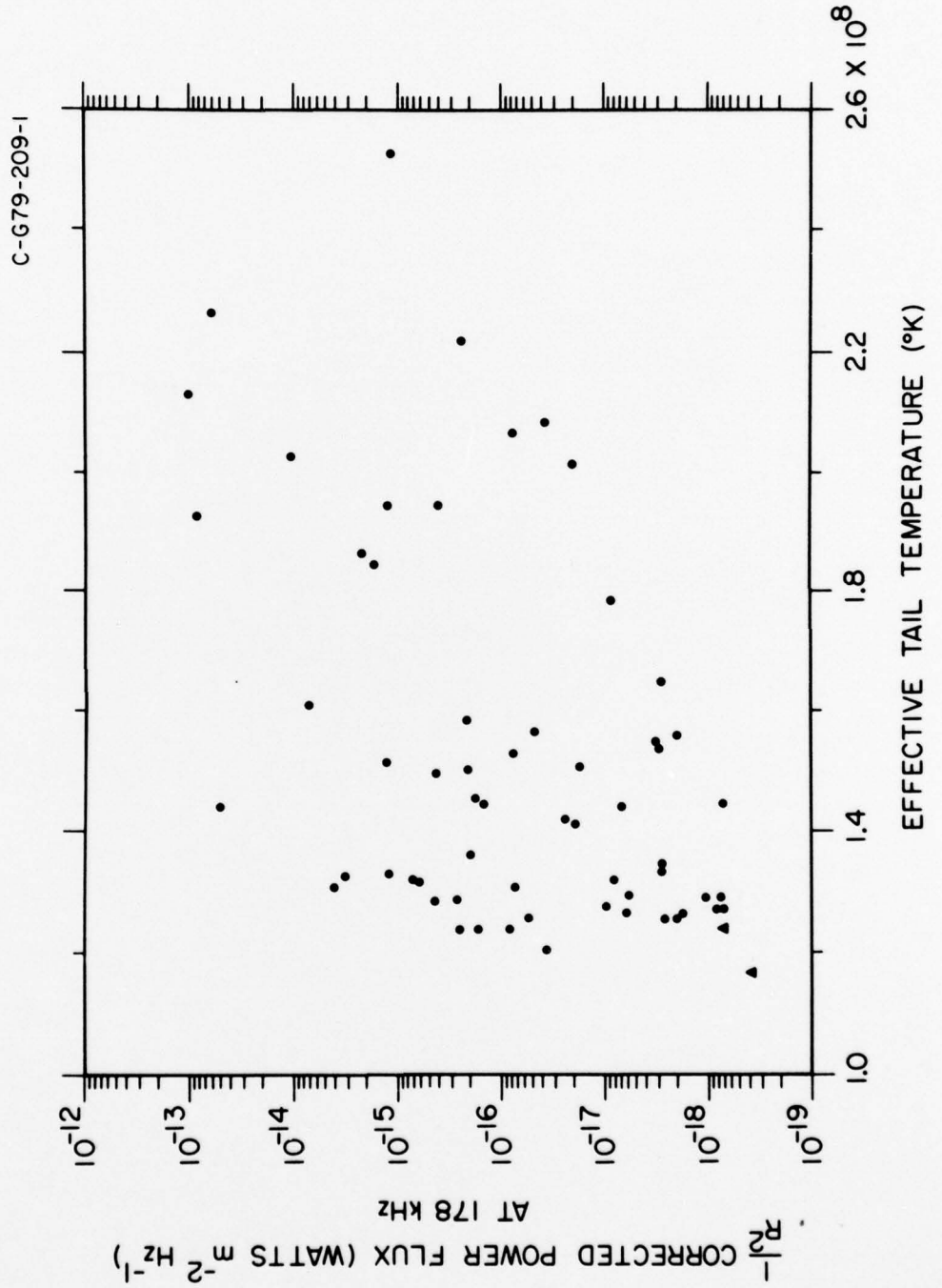
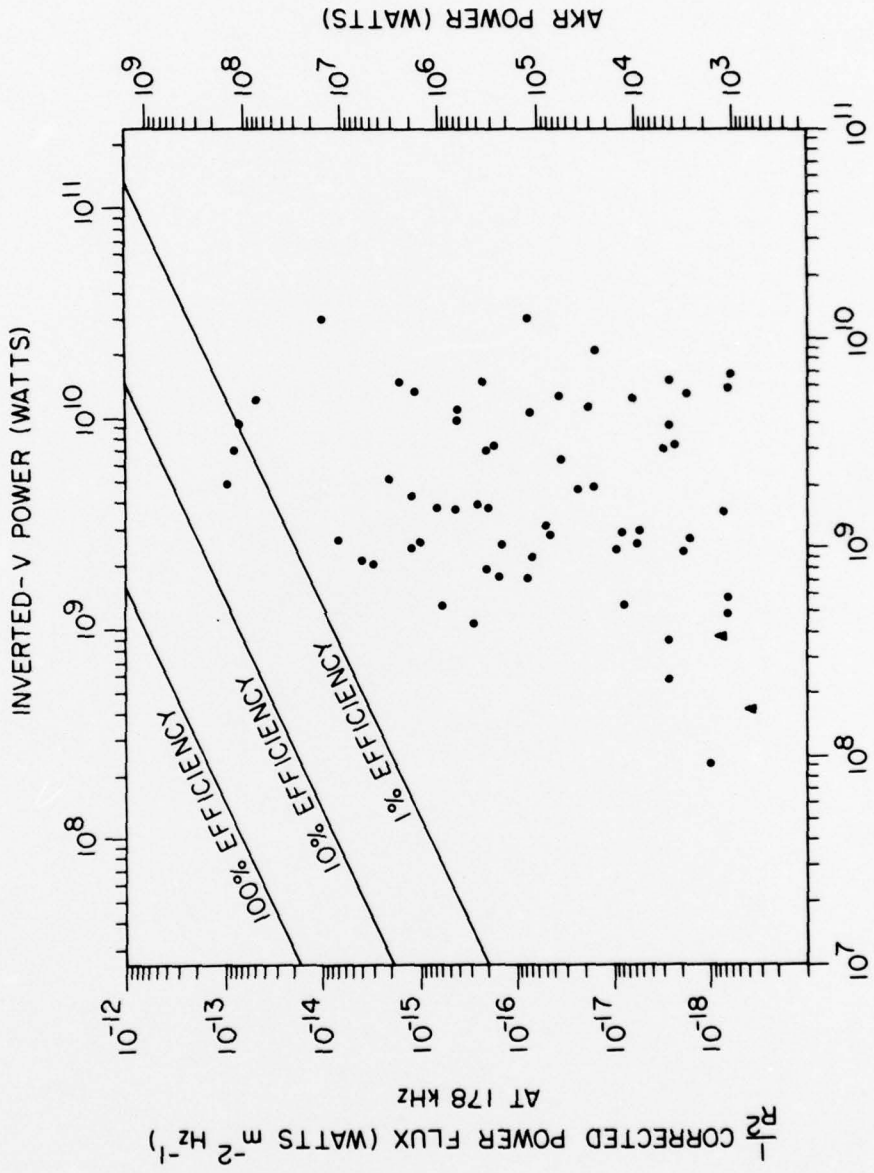


Figure 4

C-678-1011-3



INVERTED-V ENERGY FLUX (keV SEC⁻¹ CM⁻² STER⁻¹)
INTEGRATED FROM 0.2 keV TO 25 keV

Figure 5

C-679-222

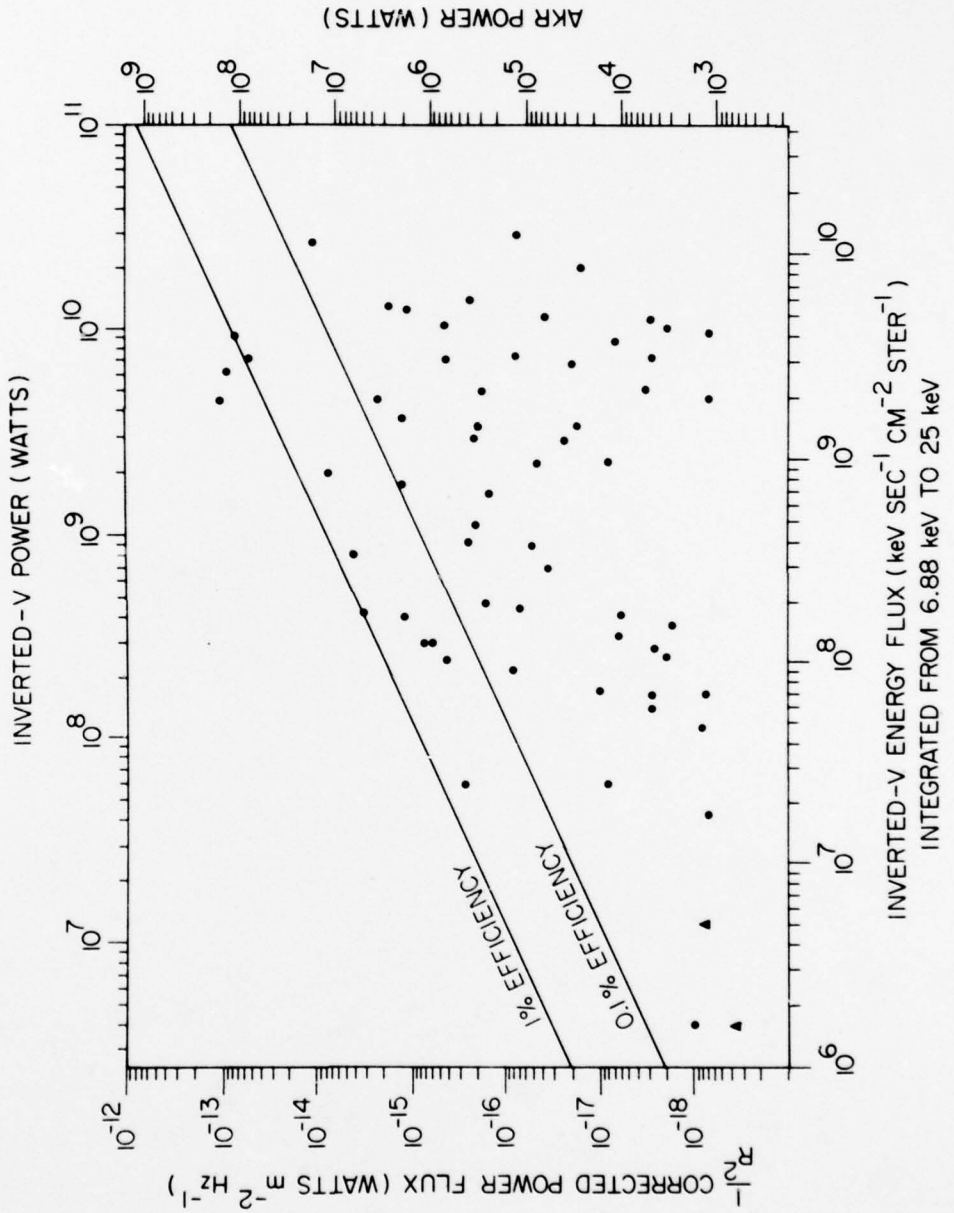


Figure 6